phycology

MDPI

Article

Photobiological and Biochemical Characterization of Conchocelis and Blade Phases from *Porphyra linearis* (Rhodophyta, Bangiales)

Débora Tomazi Pereira * and Félix L. Figueroa

Experimental Center Grice Hutchinson, Andalusian Institute of Blue Biotechnology and Development (IBYDA), Malaga University, Lomas de San Julián, 2, 29004 Malaga, Spain; felixlfigueroa@uma.es

* Correspondence: debora.tomazi@uma.es; Tel.: +34-634119406

Abstract: *Porphyra* specimens are red macroalgae with significant economic importance for food and pharmaceutical industries due to their physiological activities resulting from their bioactive compounds (BACs). Due to its economic importance, this research aimed to characterize the photosynthetic and biochemical aspects of the conchocelis and blade phases of *Porphyra linearis* to understand and help improve production of this algae. The algae were cultured for 7 days with nutrients for blade phase measurements, while another portion was cultured without nutrients for 21 days to release carpospores, which were cultivated for 4 months. For both phases, the content of BACs (chlorophyll *a*, carotenoids, phycobiliproteins, phenols, carbohydrates, proteins, mycosporine-like amino acids), antioxidant activity, and photosynthetic parameters were analyzed. Most of the parameters showed the blade phase had better results than conchocelis, except for carbohydrates. Phycobiliproteins showed no statistical differences between the phases. These findings highlight that conchocelis is not a good BACs source compared to the blade phase, but it is a crucial phase in the life cycle of *Porphyra*. Understanding the key parameters for maintaining the cultivation of conchocelis stocks for the development of the blade phase is a way to produce macroscopic biomass of this economically important algae throughout the year.

Keywords: bioactive compounds; macroscopic phase; microscopic phase; photosynthesis

Academic Editor: Pilar García-Jiménez

Received: 28 January 2025
Revised: 25 February 2025
Accepted: 27 February 2025
Published: 28 February 2025

Citation: Pereira, D.T.; Figueroa, F.L. Photobiological and Biochemical Characterization of Conchocelis and Blade Phases from *Porphyra linearis* (Rhodophyta, Bangiales). *Phycology* **2025**, *5*, 9. https://doi.org/10.3390/phycology5010009

1. Introduction

Porphyra sensu lato species are red macroalgae holding significant economic value, responsible for generating billions of dollars annually due to sushi production. These algae grow in the supralittoral zone, showing resistance and resilience to environmental stressors such as high light intensity, osmotic stress, and desiccation [1,2]. The life cycle of *Porphyra* is characterized by an alternation of generations between a macroscopic phase (gametophytes), which are haploid, that occurs during cold temperature seasons and consists of a single cell layer and take on a blade shape, and a microscopic phase (sporophytes), which are diploid and occurs during warm temperature seasons [3]. Each generation releases different types of spores; gametophytes produce carpospores, leading to the 2n phase named conchocelis phase, while sporophytes release conchospores, initiating the n phase [3,4].

Porphyra has emerged as an algae of significant research interest due to its richness in iron, proteins, and vitamins B and C [3], establishing it as the world's most consumed and cultured red algae and a key player in the food sector [5]. Moreover, *Porphyra* is enriched

with bioactive compounds (BACs) as mycosporine-like amino acids and pophyrans, exhibiting a spectrum of beneficial health effects, such as antiviral, anticancer, anticoagulant, and antioxidant properties, immune system enhancement, and photoprotection [6–10].

The photosynthetic behavior and biochemical composition of *Porphyra* in the blade phase are well-documented [11–18]; however, these parameters are less studied in the conchocelis phase, since this phase is microscopic and complex to maintain [19–21]. The species *Porphyra linearis* Greville is common and abundant in the coastal waters of the Iberian Peninsula, making its collection easy during the winter months in this region. According to FAO Fisheries and Aquaculture, global *Porphyra* production was nearly 1 million tons in 2000, increasing to 3 million tons by 2020. Additionally, Future Market Insights reports that the algae products market was valued at USD 5.41 billion in 2023, and is projected to reach USD 9.15 billion by 2033, growing at a CAGR of 5.41%. Notably, the global *Porphyra* algae extract market is expected to experience substantial growth, expanding from USD 1.2 billion in 2023 to approximately USD 2.8 billion by 2032, reflecting a compound annual growth rate (CAGR) of 9.8%.

In addition to its great economic importance, *Porphyra* plays a crucial ecological role as a primary producer in marine ecosystems. As a photosynthetic organism, it contributes to oxygen production and carbon sequestration, helping to regulate atmospheric CO_2 levels. *Porphyra* also plays a key role in nutrient cycling, absorbing nitrogen and phosphorus from seawater, which supports the productivity of coastal environments and helps mitigate eutrophication [22]. Furthermore, *Porphyra* serves as an essential food source for a variety of marine organisms, including herbivorous invertebrates and fish, sustaining biodiversity. Its presence provides habitat for microorganisms and juvenile marine species, further enhancing its ecological significance [23].

However, few studies describe its composition and life cycle. Therefore, this study aimed to characterize both photosynthetically and biochemically the conchocelis phase, and compare it with blade phase, of *P. linearis*, to understand the behavior of this crucial developmental stage for the species' propagation, which could facilitate the cultivation and production of this economically and ecologically important algae. This understanding is key to evaluating its potential applications in biotechnology, aquaculture, and the food industry.

2. Materials and Methods

2.1. Biological Material and Conditions of Cultivation

The gametophytes of *P. linearis* were collected in the upper littoral area, on rocky shores completely exposed to the air during low tide, of Santa Cristina Beach (43°61′ N and 8°18′ W), Galicia, Spain, in May 2023, by the 'Porto Muiños' company. Algal thalli were transported to the University Institute of Blue Biotechnology and Development (IBYDA), of the University of Malaga (Spain), in plastic containers containing seawater inside a thermal box. In the laboratory, the thalli were washed with diluted artificial seawater (15 psu, produced through the dilution of sea salt from saline from Cadiz, Spain), and healthy portions were selected and followed for culture with artificial seawater (32 psu) and under controlled conditions: photosynthetic active radiation (PAR) of 120 µmol photons·m^{-2}·s^{-1} (White LED light, 5000 K, 54 W, NU-8416, Nuovo), temperature of 15 ± 2 °C, photoperiod of 12 h, and continuous aeration. Approximately a total of 15 g (n = 3) of the algae were cultured for 7 days with 400 µM of NO_3^- and 24 µM of PO_4^- weekly supplied for blade phase photosynthetically measurements, while another 15 g portion (n = 3) was cultured under the same conditions, but without nutrients, for 21 days. At the end of this period, the carpospores were released. A temperature of 15 °C was selected, as it represents the

average temperature during winter in southern Spain, while the light intensity was chosen based on the optimal conditions described in previous studies with *Porphyra* [24,25].

After the release, the obtained carpospores were cultivated at the culture room conditions for 4 months under controlled conditions: artificial seawater (32 psu) enriched with 200 µM of NO_3^- and 12 µM of PO_4^- weekly supplied (no water change), PAR of 15 µmol photons·m^{-2}·s^{-1}, temperature of 25 ± 2 °C, and a photoperiod of 12 h. A temperature of 25 °C was selected, as it represents the average temperature during summer in southern Spain, while the light intensity was chosen based on the optimal conditions described in a previous study with *Porphyra*'s conchocelis phase [26].

At the end of the seventh day for the blade phase and the fourth month for the conchocelis phase of culture, photosynthesis measurements were performed in samples of all replicates (n = 3), and after this, the samples were frozen at −80 °C for the extraction of the metabolites.

2.2. Light Microscopy

After the culture period, the mature regions (edge of the thallus) were extended between slide and coverslip to observe the release of carpospores, and observed under a light microscope (Leica DME, Wetzlar, Germany) equipped with a Leica ICC50 W camera. At the end of the fourth month of culture, fresh material was extended between the slide and coverslip and observed under a light microscope equipped with a camera. The software LAS-EZ (Leica) (version 3.4) was used for the final image processing.

2.3. Pigment Lipophilic Quantification

The extractions for the measurement of concentrations of lipophilic pigments (chlorophyll *a* and carotenoids) were performed with 50 mg of fresh conchocelis and 500 µL of extraction solvent (methanol 100%), and 100 mg of fresh blade and 1 mL of extraction solvent. After the extraction solvent was added to the algal biomass, they were macerated for 30 s using an UltraTurrax® (T25, IKA, Berlin, Germany) (18,000 rpm) and then subjected to extraction at 4 °C for 3 h. Following extraction, the samples were centrifuged at 4500 rpm (2721.6× *g*), and the supernatant was collected.

The determination of pigments concentrations was carried out according to Gheysen et al. [27]. Approximately 500 µL of the algal extract was filtered through a 0.2 µm membrane before chromatographic analysis using an HPLC system (Waters 600, Waters Chromatography S.A, Madrid, Spain) with a Diode-Array Detection (DAD) detector. The pigments separation was performed by injecting 80 µL of extract algal into a Zorbax® SB-C8 column (5 µm; 150 mm length and 4.6 mm diameter—Agilent), was kept at 30 °C and the samples at 5 °C. The mobile phases were methanol:ammonium acetate buffer (80:20, pH 7.2, 0.5 M), acetonitrile:ultra-pure water (90:10), and ethyl acetate, with a flow rate of 0.7 mL· min^{-1}, and each run took 33 min. Pigments were detected at 444, 450, and 644 nm. Purified pigments were used as standards. The quantification was performed using a standard curve (Chlorophyll *a*: 0.25 to 1.5 mg·L^{-1}—R^2 = 0.99; y = 178.52x − 9.97; Lutein: 0.13 to 1 mg·L^{-1}—R^2 = 0.97; y = 797.1x − 50.372; β-carotene: 0.19 to 1.5 mg·L^{-1}—R^2 = 0.99; y = 623.36x + 43.041), and were expressed in mg per g of DW.

2.4. Hydrophilic Bioactive Compounds Extraction

In an Eppendorf tube, the extractions of BACs were performed from 50 mg of fresh conchocelis and 1 mL of extraction solvent (distilled water), and 500 mg of fresh blade and 5 mL of extraction solvent. After the extraction solvent was added to the algal biomass, they were macerated for 30 s using an UltraTurrax® (18,000 rpm) and then subjected to extraction at 80 °C for 1.5 h. Following extraction, the samples were centrifuged at 4500 rpm (2721.6× *g*), the supernatant was collected, and the algal extracts were prepared

for the measurement of concentrations of BACs (phycobiliproteins, phenols, proteins, carbohydrates, and mycosporine-like amino acids (MAAs)) and antioxidant activity.

2.5. Total Soluble Phycobiliproteins

The determination of phycobiliprotein concentrations [phycocyanin (PC), and phycoerythrin (PE)] was performed using a UV-visible spectrophotometer (Shimadzu UV-2600, λ = 564, 618, and 730 nm), following the formulas described by Sampath–Wiley and Neefus [28]. The analyses were conducted in triplicates, and the results were expressed in mg of pigments per g of dry weight (DW).

2.6. Total Soluble Phenols

The analysis of phenols was carried out using the spectrophotometric Folin–Ciocalteu method based on Folin and Ciocalteau [29]. Aliquots of 100 µL from the diluted algal extracts were added to 700 µL distilled water, 50 µL of the Folin–Ciocalteu reagent (Sigma-Aldrich), and 150 µL of 20% sodium carbonate, and incubated for 2 h at 4 °C. Subsequently, readings were taken at 760 nm using a UV–visible spectrophotometer. The quantification of total phenols was determined using a standard curve of gallic acid (1 to 100 µg·mL^{-1}—R^2 = 0.99; y = 0.00774x). The analyses were performed in triplicate, and the results were expressed in mg of gallic acid per g of DW.

2.7. Total Soluble Carbohydrates

The analysis of carbohydrates was carried out using the spectrophotometric method based on Umbreit and Burris [30]. Aliquots of 500 µL from the diluted algal extracts were added to 1 mL anthrone 0.2% (*w*/*v*). The samples were subjected to a dry bath at 100 °C for 3 min to carry out the reaction and proceeded to be read on a UV-visible spectrophotometer at 630 nm. The quantification of total carbohydrates was determined using a standard curve of glucose (25 to 200 µg·mL^{-1}—R^2 = 0.99; y = 0.01109x). The analyses were performed in triplicate, and the results were expressed in mg of glucose per g of DW.

2.8. Total Soluble Proteins

The analysis of proteins was carried out using the spectrophotometric Bradford method based on Bradford [31]. Aliquots of 50 µL from the algal extracts were added to 750 µL phosphate buffer (0.1 M, pH 6.5) and 200 µL of the Bradford reagent (BioRad, Hercules, CA, USA) and incubated for 15 min at room temperature. Subsequently, readings were taken at 595 nm using a UV-visible spectrophotometer. The quantification of total proteins was determined using a standard curve of bovine serum albumin (Sigma-Aldrich, St. Louis, MO, USA) (4 to 60 µg·mL^{-1}—R^2 = 0.99; y = 0.0244x). The analyses were performed in triplicate, and the results were expressed in mg of bovine albumin per g of DW.

2.9. Mycosporine-like Amino Acids (MAAs)

The determination of MAAs' concentrations was carried out according to Peinado et al., [32], with modifications of Chavez-Peña [33]. Approximately 500 µL of algal extracts was filtered through a 0.2 µm membrane before chromatographic analysis using a HPLC system (1260 Agilent InfinityLab Series, Santa Clara, CA, USA) with a Diode-Array Detection (DAD) detector. The MAAs separation was performed by injecting 10 µL of extract algal into a C8 Luna Column (5 µm, 250 mm length, 4.6 mm diameter; Phenomenex, Aschaffenburg, Germany), using an isocratic run containing 1.5% aqueous methanol (*v*/*v*) plus 0.15% acetic acid (*v*/*v*) in MiliQ water as the mobile phase, with a flow rate of 0.5 mL· min^{-1}, and each run took 30 min. MAAs were detected at 320 and 330 nm. Isolated MAAs through High Performance Countercurrent Chromatography (HPCCC) were used as standards [34].

The quantification was performed using published molar extinction coefficients (ε) of the different MAAs [35,36] and were expressed in mg per g of DW.

2.10. Antioxidant Activity

Antioxidant capacity was determined by the ABTS radical scavenging assay. Firstly, the radical cation $ABTS^{+\bullet}$ was prepared by mixing 7 mM of ABTS (2,2′-azino-bis (3-ethylbenzothiazoline-6-sulphonic acid; Sigma-Aldrich) and 2.45 mM of potassium persulfate ($K_2S_2O_8$) in a sodium phosphate-buffer solution (0.1 M, pH 6.5). The mixture was incubated in darkness at room temperature for 16 h for the complete formation of the radical. For the reaction, the $ABTS^{+\bullet}$ was diluted with phosphate buffet until absorbance at 727 nm were 0.75 ± 0.05. The assay was performed by adding 950 µL of the diluted $ABTS^{+\bullet}$ solution and 50 µL of diluted algal extract, according to Re et al. [37]. The samples were shaken, and absorbance was recorded by a UV-visible spectrophotometer at 727 nm at the beginning of the reaction (DOi) and after 8 min of incubation (DOf). The percentage of antioxidant activity (AA%) was calculated according to the formula:

$$AA\% = [(absDOi - absDOf)/absDOi] \times 100$$

The antioxidant compounds concentration was calculated using a standard curve of Trolox (6-hydroxy-2,5,7,8-tetramethylchroman-2-carboxylic acid), (Sigma-Aldrich) (20 to 100 $\mu g \cdot mL^{-1}$—$R^2 = 0.99$; y = 15.8928x), and the results expressed in µmol of Trolox equivalent antioxidant capacity (TEAC) per g of DW.

2.11. Photosynthesis and Energy Dissipation as In Vivo Chlorophyll a Fluorescence

2.11.1. In Vivo Measurements

To assess the actual effects of the different cultivation conditions and stages of life, in vivo measurements were conducted. In vivo chlorophyll *a* fluorescence was measured in situ, directly under the cultivation conditions in the culture chambers. To achieve this, saturating pulses (>3000 µmol photons$\cdot m^{-2} \cdot s^{-1}$) were applied to algal thalli (three replicates per cylinder) during the dark phase of the daily photoperiod. This approach aimed to quantify three distinct fluorescence parameters: the basal fluorescence (F_0), the steady-state fluorescence (F_t), and the maximal fluorescence (F_m, which is measured in dark-adapted samples or F_m' in light-acclimated samples) using a portable pulse amplitude modulated fluorometer (Diving-PAM II (Walz®, Germany)). The optimal or maximal quantum yield (F_v/F_m) and the effective quantum yield (Y(II)) were assessed at 7 days of culture for blade phase, and 4 months for the conchocelis phase. Calculations for F_v/F_m and Y(II) were conducted using their respective standard formulas:

$$F_v/F_m = (F_m - F_o)/F_m$$

$$Y(II) = (F_m' - F_t)/F_m'$$

2.11.2. Ex Vivo Measurements

To assess the maximum photosynthetic capacity of each stage of life from *P. linearis* under controlled laboratory conditions, ex vivo measurements were conducted. The electron transport rate (ETR) was determined in the laboratory (ex situ) through rapid light curves (RLCs) by exposing samples to thirteen ascending irradiances, ranging from 0 to 875 µmol photons$\cdot m^{-2} \cdot s^{-1}$ for the conchocelis phase and 0 to 1500 µmol photons$\cdot m^{-2} \cdot s^{-1}$ for the blade phase, of actinic red light (LEDs) provided the Diving-PAM II. After 30 s of incubation at each irradiance level, a saturating pulse was applied to the samples. At each irradiance level of the RLCs, different parameters were calculated, including the effective quantum

yield (Y(II)), ETR, and two different types of yield losses: the yield for non-photochemical quenching (Y(NPQ)) calculated as $(F_t/F_m') - (F_t/F_m)$ and the yield for non-regulated energy dissipation (Y(NO)) calculated as F_t/F_m. Additionally, nonphotochemical quenching (NPQ) was calculated using the formula Y(NPQ)/Y(NO). The energy dissipation rate (EDR) was also evaluated. The ETR [38] and EDR [39] were calculated as follows:

$$\text{ETR } (\mu\text{mol } e^- \text{ m}^{-2}\text{s}^{-1}) = \text{Y(II)} \times E_{PAR} \times A \times F_{II}$$

$$\text{EDR } (\mu\text{mol photons}\cdot\text{m}^{-2}\cdot\text{s}^{-1}) = (\text{Y(NO)} + \text{Y(NPQ)}) \times E_{PAR} \times A \times F_{II}$$

where Y(II) is the effective quantum yield, Y(NO) is the yield loss related to passive thermal dissipation, and Y(NPQ) is the yield loss related to the photoregulated process; E_{PAR} is the incident PAR irradiance expressed in μmol photos·m^{-2}·s^{-1}, A is the absorptance that was calculated as $A = 1 - (E_t/E_0)$ (E_t is the irradiance that pass through the thallus and E_0 is the emitted irradiance), and F_{II} is the fraction of chlorophyll *a* associated with PSII, being 0.15 in red macroalgae [40,41]. The obtained ETR and NPQ vs. irradiance curves were fitted according to Eilers and Peeters [42] and other parameters were obtained: photosynthetic efficiency of ETR (α_{ETR}), maximal ETR (ETR_{max}), saturated irradiance of ETR (Ek_{ETR}) and NPQ (Ek_{NPQ}) and optimal irradiance ($Eopt_{ETR}$), respectively. The Ek_{ETR} was subtracted from the Eopt values, and Ek_{NPQ} was subtracted from the Ek_{ETR} to know the range of intensity in which the photosynthesis is maintained in steady state.

2.12. Statistical Analysis

The data passed the Shapiro–Wilk normality test and the Bartlett test for homogeneity of variances, and all samples were within the normal range ($p \geq 0.05$) and exhibited homoscedasticity ($p \leq 0.05$). Afterwards, the data were analyzed by the independent-samples *t*-test ($p \leq 0.05$), and Cohen's d test, to assess the effect size of the difference between the two groups. Statistical analyses were performed using the Statistica software package (Release 10.0).

3. Results

3.1. Microscopic Morphology

After 21 days of cultivation without nutrients, the thallus, which initially exhibited a brownish coloration when maintained after seven days of cultivation with nutrients, turned greenish, and the thallus edges became reddish, indicating the formation of mature reproductive cells. Carpospores were released and, upon adhesion, began polarization to form the germ tube. After 4 months of culture, the carpospores grew and developed into the conchocelis phase, characterized by filaments emerging from the carpospores, which displayed a reddish coloration (Figure 1).

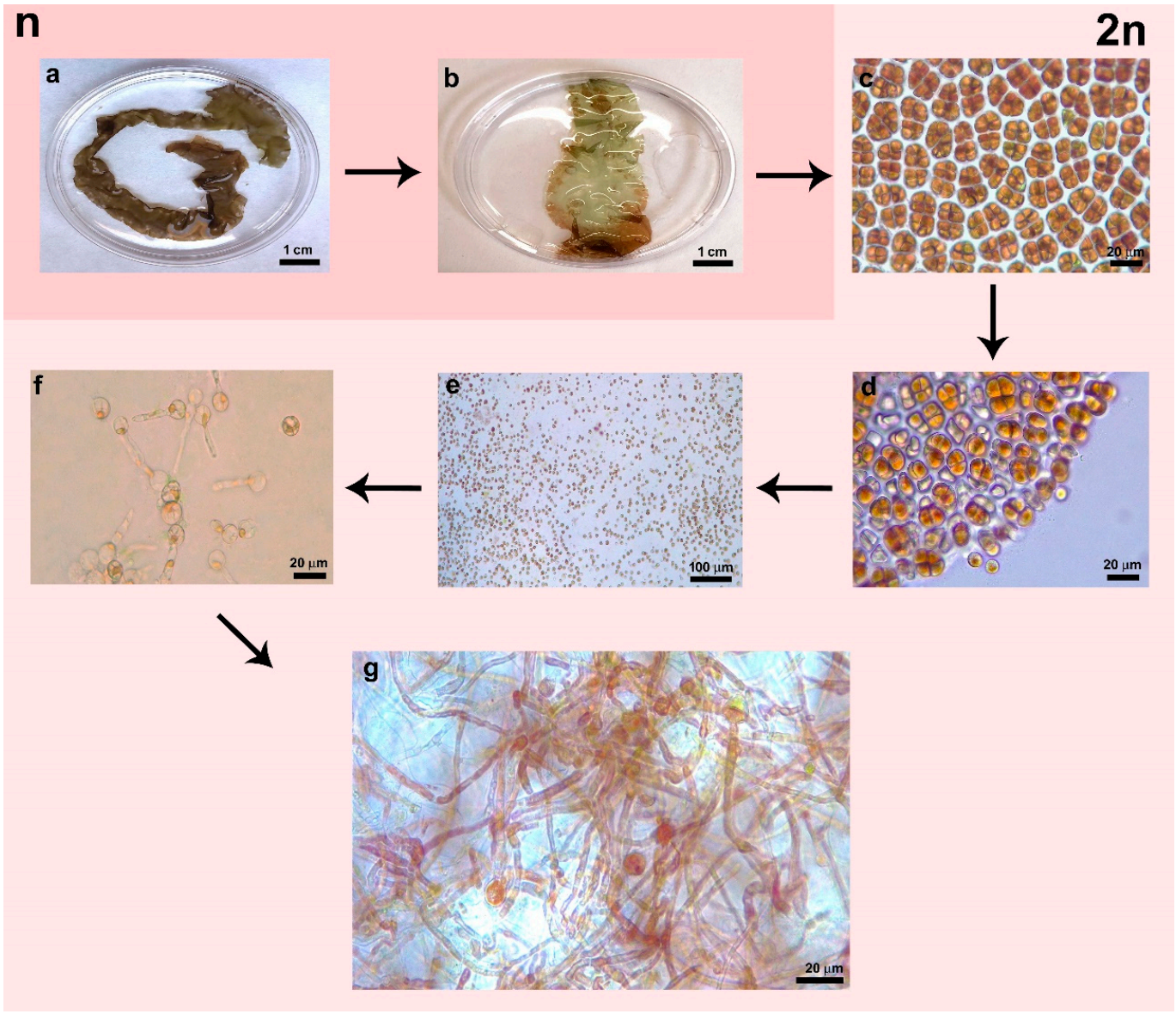

Figure 1. Biphasic and heteromorphic life cycle of *P. linearis* observed under light microscopy. (**a**). non-fertile blade phase; (**b**). fertile blade phase (reddish areas), (**c**). carposporangia; (**d**). release of carpospores; (**e**). carpospores; (**f**). carpospores with a germination tube, forming the conchocelis phase; (**g**). conchocelis phase after 4 months of culture.

3.2. Concentrations of Lipophilic Photosynthetic Pigments: Chlorophyll a and Carotenoids

Regarding the lipophilic compounds, it was observed that chlorophyll *a* (d = 68.00, $p \leq 0.0001$) and lutein (d = 7.02, $p \leq 0.05$) levels were significantly higher in the blade phase compared to the conchocelis phase. Specifically, chlorophyll *a* exhibited approximately twice the amount, while lutein showed a one and a half times increase in concentration (Figure 2). The relation Lutein/Chl *a* was 0.44 and 0.57 in blade and conchocelis, respectively.

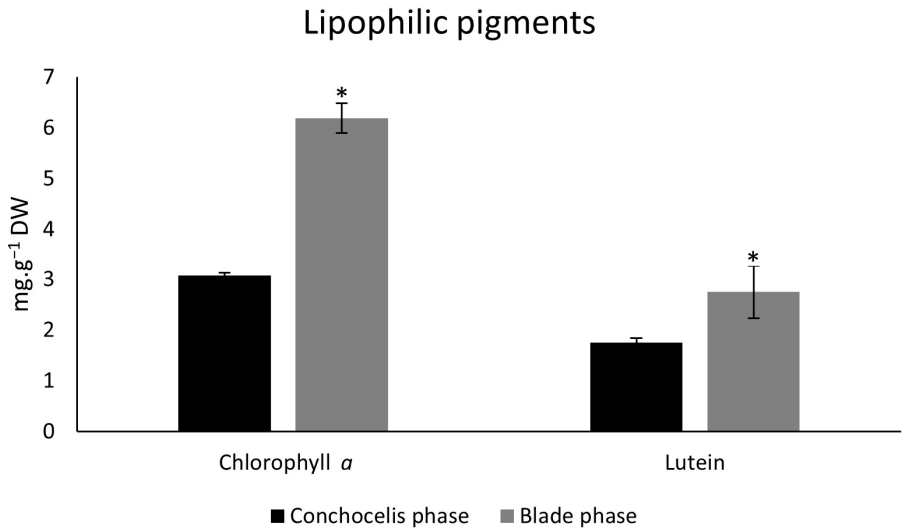

Figure 2. Concentrations of lipophilic pigments (chlorophyll *a* and lutein) (mg·g^{-1} dry weight) in conchocelis (after four months of culture) and blade phase (after seven days of culture) of *P. linearis* (n = 3; mean ± SD). Asterisks indicate significant differences according to the independent *t*-test analysis (between conchocelis and blade phases) ($p \leq 0.05$).

3.3. Concentrations of Hydrophilic Bioactive Compounds and Antioxidant Activity

Focusing on the hydrophilic compounds within the phycobiliprotein group, two pigments, phycoerythrin (PE) and phycocyanin (PC), were quantified. After four months of cultivating the conchocelis phase, PE was found in higher concentration than PC, resulting in a stoichiometry of 3.08 (PE:PC). For the blade phase, PE was also present in greater quantity compared to PC, exhibiting a stoichiometry of 2.20 (PE:PC). The PE:PC ratio was statistically higher in the conchocelis samples ($d = -12.22$, $p \leq 0.02$). On the other hand, no statistical difference was observed in the PE content between the two phases, and the same pattern was observed for the PC content (Table 1 and Table S1).

Table 1. Concentrations of hydrophilic bioactive compounds (phycobiliproteins (PE: phycoerythrin) and PC: phycocyanin, as well as PE:PC ratio); soluble total phenols, proteins and carbohydrates (mg·g^{-1} dry weight) and concentrations of antioxidant agents (µmol of Trolox (TEAC)·g^{-1} dry weight) in conchocelis (after four months of culture) and blade phase (after seven days of culture) of *P. linearis* (n = 3; mean ± SD). Asterisks indicate significant differences according to the independent *t*-test analysis (between conchocelis and blade phases) ($p \leq 0.05$).

Hydrophilic Compounds	Conchocelis Phase	Blade Phase
Phycoerythrin (PE)	2.00 ± 0.32	1.96 ± 0.33
Phycocyanin (PC)	0.65 ± 0.09	0.89 ± 0.17
PE:PC	3.08 ± 0.10 *	2.20 ± 0.36
Soluble Total Phenols	1.34 ± 0.13	15.93 ± 1.48 *
Soluble Proteins	0.84 ± 0.11	1.39 ± 0.16 *
Soluble Total Carbohydrates	76.16 ± 3.62 *	49.25 ± 2.63
ABTS test	4.45 ± 0.72	23.37 ± 1.68 *

Regarding the total soluble phenols (d = 100.67, $p \leq 0.0001$) and soluble proteins (d = 29.74, $p \leq 0.01$), the blade phase exhibited a significantly higher amount, approximately ten and one and a half times, respectively, compared to the conchocelis phase. However, considering the amount of total soluble carbohydrates ($d = -2.69$, $p \leq 0.001$), a significant statistical difference was noted, where the conchocelis phase had the higher concentration,

approximately twice that of the blade phase. Finally, the antioxidant activity was significantly higher (d = 11.38, $p \leq 0.0001$), statistically, in the blade phase, approximately five times, when compared to the conchocelis phase (Table 1).

Within the context of hydrophilic compounds, HPLC analysis identified the presence of only one type of MAA, shinorine, in the conchocelis phase, while for the blade phase, three types were identified: palythine, shinorine, and Porphyra-334. Shinorine is the only MAA common between the two phases and was found in higher quantity, with a statistically significant difference, in the blade phase (d = 25.01, $p \leq 0.003$). The total MAA content was slightly over a thousand times higher in the blade phase compared to the conchocelis phase (Table 2).

Table 2. Concentrations of hydrophilic bioactive compounds (mycosporine-like amino acids (palythine, shinorine, Poprhyra-334, and sum of all identified MAAs)) (mg·g^{-1} dry weight) in conchocelis (after four months of culture) and blade phase (after seven days of culture) of *P. linearis* (n = 3; mean ± SD). Asterisks indicate significant differences according to the independent t-test analysis (between conchocelis and blade phases) ($p \leq 0.05$), and the dash (-) indicates that MAA was not detected.

MAAs (mg·g^{-1} DW)	Conchocelis Phase	Blade Phase
Palythine	-	0.01 ± 0.0001
Shinorine	0.02 ± 0.001	1.20 ± 0.31 *
Porphyra-334	-	19.04 ± 4.48
Total MAAs	0.02	20.25

3.4. Photosynthetic Parameters (In Situ and Ex Situ)

The $ETR_{in\ situ}$ (d = 1603.25, $p \leq 0.0001$) and ETR_{max} (ex situ) (d = 76.40, $p \leq 0.0001$) were higher and showed statistical differences in samples derived from the blade phase compared to those from the conchocelis phase. Specifically, the $ETR_{in\ situ}$ was approximately six times higher, while the ETR_{max} was about four times in blade phase compared to conchocelis ones. When compared within samples from the same phase, ETR_{max} was found to be higher than $ETR_{in\ situ}$ (Figure 3).

After performing rapid light curves (RLCs) on conchocelis and blade phases of *P. linearis*, some photosynthetic parameters were analyzed ex vivo. The Fv/Fm (d = 346.88, $p \leq 0.001$) was higher in the blade phase compared to the conchocelis phase, showing a significant statistical difference with an approximate two times of increase. The α_{ETR} did not exhibit any statistical difference between the two phases analyzed. However, the Ek_{ETR} (d = 1.45, $p \leq 0.0001$), $Eopt_{ETR}$ (d = 1.67, $p \leq 0.0001$), NPQ_{max} (d = 25.57, $p \leq 0.003$), and Ek_{NPQ} (d = −0.56, $p \leq 0.0001$) displayed statistical differences between the two phases, with the blade phase showing increases of approximately 3.5, 2.8, and 4.7 times in the first three parameters, and a decrease of 1.9 times in the last parameter (Table 3).

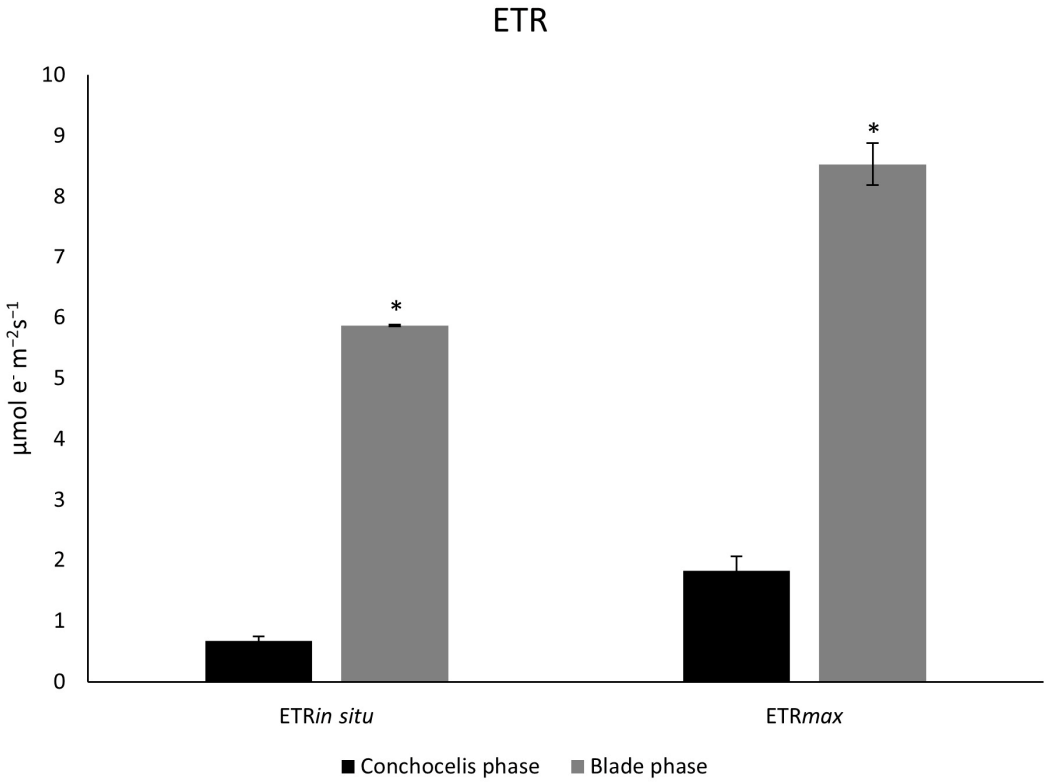

Figure 3. Electron transport rate in situ ($ETR_{in\ situ}$—µmol e^- $m^{-2}s^{-1}$) and maximal ETR under ex situ measurements (ETR_{max}—µmol e^- $m^{-2}s^{-1}$) in conchocelis (after four months of culture) and blade phase (after seven days of culture) of *P. linearis*. Values are calculated as mean ± standard deviation (SD) (n = 3). Asterisks indicate significant differences according to the independent *t*-test analysis (between conchocelis and blade phases) ($p \leq 0.05$).

Table 3. Photosynthetic parameters (optimal quantum yield (F_v/F_m), αETR (photosynthetic electron transport rate efficiency), Ek_{ETR} (ETR saturated irradiance—µmol photons $m^{-2}s^{-1}$), $Eopt_{ETR}$ (ETR optimal irradiance—µmol photons $m^{-2}s^{-1}$), NPQ_{max} (NPQ maximum), Ek_{NPQ} (NPQ saturated irradiance—µmol photons $m^{-2}s^{-1}$), and difference between $Eopt_{ETR}$ and Ek_{ETR}, and between Ek_{NPQ} and Ek_{ETR}—µmol photons $m^{-2}s^{-1}$) obtained after the adjustment of the rapid light curves (RLCs) in conchocelis phase (after four months of culture) and blade phase (after seven days of culture) of *P. linearis*. Values are calculated as mean ± standard deviation (SD) (n = 3). Asterisks indicate significant differences according to the independent *t*-test analysis (between conchocelis and blade phases) ($p \leq 0.05$).

Photosynthetic Parameters	Conchocelis Phase	Blade Phase
F_v/F_m	0.490 ± 0.02	0.656 ± 0.03 *
α_{ETR}	0.04 ± 0.002	0.06 ± 0.004
Ek_{ETR}	43.16 ± 2.95	153.34 ± 12.13 *
$Eopt_{ETR}$	193.72 ± 18.78	542.34 ± 8.06 *
$Eopt_{ETR}$—Ek_{ETR}	144.09 ± 10.99	388.87 ± 11.71 *
NPQ_{max}	0.30 ± 0.05	1.43 ± 0.29 *
Ek_{NPQ}	634.23 ± 24.76 *	336.36 ± 21.04
Ek_{NPQ}—Ek_{ETR}	591.07 ± 32.12 *	182.90 ± 20.77

The range between $Eopt_{ETR}$ and Ek_{ETR} was significantly greater in samples from the blade phase, with a difference of approximately 244 µmol photons·m^{-2}·s^{-1}, whereas the

range between Ek_{NPQ} and Ek_{ETR} was significantly greater in samples from the conchocelis phase, with a difference of 408 µmol photons·m^{-2}·s^{-1} (Table 3).

Selecting irradiance intensities similar to the cultivation of each phase (12 µmol photons·m^{-2}·s^{-1} for conchocelis and 124 µmol photons·m^{-2}·s^{-1} for the blade phase), the median irradiance of the rapid light curve (RLC) (110 µmol photons·m^{-2}·s^{-1} for conchocelis and 625 µmol photons·m^{-2}·s^{-1} for the blade phase), and the maximum irradiance of the RLC (873 µmol photons·m^{-2}·s^{-1} for conchocelis and 1492 µmol photons·m^{-2}·s^{-1} for the blade phase), statistical differences were observed among all light intensities for both ETR and EDR. Upon calculating the ETR and EDR ratio, a consistent pattern emerged across the three intensities and the two phases analyzed. At the lowest intensity, the ratio was highest, indicating minimal light dissipation. At the median intensity, the ratio was slightly lower, demonstrating more considerable dissipation, while at the highest light intensity, the ratio was much lower, signifying extensive light dissipation (Table 4).

Table 4. Electron transport rate (ETR) and energy dissipation rate (EDR) (µmol e^- $m^{-2}s^{-1}$), and ETR:EDR ratio obtained after the adjustment of the rapid light curves (RLCs) at 12, 110, and 873 µmol photons $m^{-2}s^{-1}$ in conchocelis phase (C) (after four months of culture) and at 124, 625, and 1492 µmol photons $m^{-2}s^{-1}$ in blade phase (B) (after seven days of culture) of *P. linearis*. Values are calculated as mean ± standard deviation (SD) (n = 3). Asterisks indicate significant differences according to the independent t-test analysis (between conchocelis and blade phases) ($p \leq 0.05$).

Photosynthetic Parameters	Conchocelis Phase	Blade Phase
$ETR_{12C,124B}$	0.46 ± 0.11	4.92 ± 0.22 *
$EDR_{12C,124B}$	1.01 ± 0.03	8.09 ± 0.21 *
$ETR_{12C,124B}$:$EDR_{12C,\ 124B}$	0.46	0.61
$ETR_{110C,625B}$	1.68 ± 0.25	8.48 ± 0.33 *
$EDR_{110C,625B}$	11.61 ± 0.40	59.47 ± 1.13 *
$ETR_{110C,625B}$:$EDR_{110C,\ 625B}$	0.14	0.14
$ETR_{873C,1492B}$	1.08 ± 0.20	6.49 ± 0.17 *
$EDR_{873C,1492B}$	113.27 ± 11.15	158.71 ± 10.11 *
$ETR_{873C,1492B}$:$EDR_{873C,1492B}$	0.01	0.04

4. Discussion

The present study characterized both photosynthetically and biochemically the two phases present in the life cycle of *P. linearis*, the blade/macroscopic phase; and the conchocelis/microscopic phase, and differences as well as some similarities were observed between them.

It is known that chlorophyll *a* is a primary metabolite and the principal photosynthetic pigment in algae, and it is the most protected pigment in the antenna complex [43,44]. Due to the vital importance of this pigment, its higher quantity among the pigments found in both phases of *P. linearis* is justified, although the blade phase showed a higher concentration. Similar results to those found in the present study were observed in the blade phase in *P. columbina* (4.0 mg· g^{-1}) [32], *P. umbilicales* (4.3 mg· g^{-1}) [12], *P. haitanensis* (4.5 mg· g^{-1}) [45], and *P. linearis* (approximately 5 mg· g^{-1}) [46], and in the conchocelis phase in *P. abbottae* (4 mg· g^{-1}) [47] and in *P. haitanensis* (2 mg· g^{-1}) [45]. The macroscopic phase grows, is cultivated, and exhibits a higher Ek_{ETR} under high light intensities, whereas the conchocelis phase under lower intensities. The Ek_{ETR} is the light intensity at which the ETR curve begins to stabilize, representing the optimal radiation for cultivation and efficient utilization of light energy. In nature, the development of the conchocelis phase

occurs at greater depths, especially adhering to shells [3], indicating environments with lower light levels, justifying the lower Ek_{ETR} in the conchocelis phase compared to the blade phase.

Carotenoids are secondary metabolites that, besides assisting in the photosynthesis process, can also act as antioxidant agents [48,49]. In both phases of the algae, the lutein carotenoid was detected. Lutein is considered necessary for the folding of the antenna complexes [50,51], being directly affected by light intensity [52], which explains the higher amount of lutein in the blade phase found in this study. Additionally, lutein is an antioxidant agent [53], and the more available light during cultivation, the higher the ETR and consequently the greater the chances of creating reactive oxygen species (ROS), explaining the higher concentration of lutein in the macroscopic phase of *P. linearis*. Other studies have reported lutein concentrations consistent with the pattern observed in the present study. *P. haitanensis* exhibited approximately 2.5 mg· g^{-1} of total carotenoids in the blade phase, while the conchocelis phase contained around 1.00 mg· g^{-1} [45]. Similarly, *P. linearis* presented a lutein concentration of 2 mg· g^{-1} in the blade phase [46]. However, in contrast to these findings, *Pyropia yezoensis* has been reported to contain more lutein in the conchocelis phase (3.5 mg· g^{-1}) compared to the blade phase (1.5 mg· g^{-1}), which differs from the results obtained in this study [54].

Phycobiliproteins are secondary pigments located in phycobilisomes in red algae that act as accessory photosynthetic pigments associated with Photosystem II composing, but they are also dissipators of excess energy [55], as well as antioxidant agents [56,57] and nitrogen reservoirs [11]. Both the macroscopic and microscopic phases showed no statistical differences in the concentrations of the two analyzed phycobiliproteins (phycoerythrin (PE) and phycocyanin (PC)). However, a lower PE:PC stoichiometry was observed in the blade phase algae, indicating a proportionally higher amount of PC relative to PE. PC is located above PE in the antenna complex and thus it is more protected [43], which may justify this small difference, as PC is more protected from oxidation and can accumulate even under higher light intensities, and/or PE is more susceptible to oxidation and degradation. The higher PE:PC ratio in the conchocelis phase compared to the blade phase indicates a higher capacity to absorb green light compared to red light. Conchocelis microscopic filaments grow normally under shade environments, i.e., canopies enriched in green light [44]. Moreover, spectral composition plays a crucial role in regulating the structure, size, and shape of phycobilisomes, influencing their light-harvesting efficiency [58,59].

A study conducted with *Nostoc sphaeroides* [60] demonstrated a similar phenomenon, where lower light intensity led to a higher PE:PC stoichiometry, while higher intensity resulted in a lower stoichiometry, even inverting the ratio.

The MAAs are secondary nitrogenous metabolites, known for their UV-absorbing and antioxidant properties [61,62]. Only one type of MAA was detected in the conchocelis phase, while three types were detected in the blade phase. Additionally, the total amount of MAAs detected was 1000 times higher in the blade phase. Naturally, as mentioned earlier, the conchocelis phase is found in more shaded areas, such as inside shells, while the blade phase is found in the intertidal zone and during low tide is fully exposed to ultraviolet radiation [3]. These natural conditions are closely linked to the production of MAAs. The quantification of MAAs in gametophytes of *Porphyra sensu lato* has been reported, ranging from 4 to 28 mg· g^{-1} [16,32,63,64]. However, no studies have described the quantification of MAAs in the conchocelis phase. In this context, Jiang and Gao [45] quantified UVA-absorbing compounds (UVACs) based on absorbance at 336 nm for the conchocelis phase and 339 nm for the blade phase. The authors found approximately 7.5 mg· g^{-1} of UVACs in gametophytes, whereas in sporophytes, the concentration was less than 0.5 mg· g^{-1} [45]. However, when measuring absorbance at this wavelength, various

compounds may interfere with the final results, in addition to MAAs, including phenols, proteins, and phycobiliproteins. However, even without quantifying MAAs separately, the significant difference in UVACs between the two phases supports the findings of the present study.

Phenols are secondary metabolites responsible for cellular antioxidation and protection against UV radiation [65], while soluble proteins are primary metabolites that perform essential functions such as structuring, signaling for growth and cell division, and also exhibit antioxidant action through enzymes like catalase, superoxide dismutase, and peroxidases [66]. These two compounds were higher in the blade phase, as it is exposed to higher light intensity when compared to the conchocelis phase, which could favor cellular oxidation. Additionally, the antioxidant response was also statistically higher in the macroscopic phase of *P. linearis*, as it is closely linked to the presence of antioxidant compounds such as MAAs, phenols, and proteins. For these two compounds, similar values have been reported in previous studies on gametophytes, with *P. linearis* presenting 2 mg· g^{-1} of phenols [46], *Porphyra* sp. containing 2.9 mg· g^{-1} of phenols [67], 2.2 mg· g^{-1} of soluble proteins [67], and 2.5 mg· g^{-1} of soluble proteins [14]. In contrast, no data on phenols and soluble proteins have been found in the literature for the conchocelis phase.

The main carbohydrates found in *Porphyra* can be classified as soluble monosaccharides, including xylose, mannose, galactose, arabinose, and glucose; a soluble polysaccharide, porphyran; and an insoluble polysaccharide, cellulose. In addition, starch, a partially soluble polysaccharide, which is the energy storage molecule [68–72]. In this study, higher concentrations of soluble carbohydrates were detected in the conchocelis phase. This microscopic phase of *Porphyra* undergoes rapid cellular growth, and soluble monosaccharides are quickly metabolized through glycolytic pathways and the Krebs cycle, generating ATP, which is essential for cell growth. Additionally, it possesses a thick cell wall containing porphyran, to aid in substrate adhesion and consequently elongation/growth of the germination tube [73]. On the other hand, the macroscopic phase will have a thick cell wall, with a high content of the sulfated polysaccharide, the porphyran, when exposed to abiotic stressors such as UV radiation, as observed in *Pyropia acanthophora* var. *brasiliensis* [15], which was not the case in the present study.

Regarding photosynthetic parameters, due to their higher pigment content, the blade phase exhibits higher measurements of $ETR_{in\ situ}$, ETR_{max}, as well as Fv/Fm, indicating a greater photosynthetic capacity. The Fv/Fm detected in the conchocelis phase in this study was approximately 0.5, similar to what Ma et al. [20] detected in the conchocelis phase of *P. yezoensis*, while Kim et al. [19] obtained close to 0.6 when the conchocelis of *P. dentata* was exposed to red and/or blue light, colors that increase the amounts of photosynthetic pigments as described for *P. umbilicalis* blade [11].

The Ek_{ETR} was approximately 3.5 times higher in the blade phase (153 µmol photons·m^{-2}·s^{-1}) compared to the conchocelis phase (43 µmol photons·m^{-2} s^{-1}), while Ek_{NPQ} was approximately 2.7 times lower in the blade phase (233 µmol photons·m^{-2}·s^{-1}) compared to the conchocelis phase (634 µmol photons·m^{-2}·s^{-1}). This indicates that the saturation irradiance is much lower in the microscopic phase, justifying its natural development in shaded environments. On the other hand, the microscopic phase can withstand high light intensities before beginning to dissipate energy, demonstrating that energy dissipation takes time to saturate. NPQ is calculated by dividing Y(NPQ) by Y(NO), indicating an algae's energy dissipation capacity. The NPQ_{max} observed in the conchocelis phase was 4.7 times lower compared to the blade phase. Lower NPQ_{max} values indicate that passive energy dissipation through heat and fluorescence, mainly due to closed PSII reaction centers (Y(NO)) [74] is greater in the microscopic phase, while in the blade phase, energy dissipation through heat via the active and regulated pathways, such as the xanthophyll cycle

(Y(NPQ)) is more relevant [75]. These results explain the high photoprotection capacity in the blade phase, as it is adapted to a more luminous habitat, whereas the conchocelis phase shows an inability to protect against photodamage caused by excess radiation. Thus, the photosynthetic pattern of conchocelis correspond to "shade type algae" since it presents lower ETR, Ek_{ETR}, $Eopt_{ETR}$, and NPQ_{max} compared to blade phase specimens, although as typical shade algae it would expected to see higher photosynthetic efficiency (α_{ETR}) than was observed.

The conchocelis phase presents a narrow range between $Eopt_{ETR}$ and Ek_{ETR}, whereas the blade phase exhibits a wider range, supporting a variety of light intensities and leading to photoinhibition at high light intensities. Additionally, the analysis of the intensity range between Ek_{NPQ} and Ek_{ETR} demonstrates the conditions under which the algae perform photosynthesis and dissipation has not yet begun. Furthermore, despite the big difference between them, this study showed the widest range between these two parameters for the conchocelis phase, while the blade phase resulted in the narrowest range.

For all three light intensities analyzed, derived from RLCs, both ETR and EDR were higher in the macroscopic phase than in the microscopic phase. However, when considering the ratio between them, a pattern emerges: at the lowest intensity, the ratio was highest, indicating minimal light dissipation; while at the highest light intensity, the ratio was much lower, signifying extensive light dissipation. The high energy dissipation in blade phase specimens, i.e., increasing EDR values with the irradiance increase and higher EDR values in blade compared to that in conchocelis phase specimens, indicates high acclimation to elevated irradiance being photoinhibition, a photoprotection mechanism that has been previously reported in *Porphyra* species [40,76–78].

In conclusion, the gametophyte/macroscopic/blade phase of *P. linearis* exhibited higher concentrations in all analyzed photosynthetic parameters and BCAs, except for phycobiliproteins, which showed no differences when compared to the sporophyte/microscopic/conchocelis phase, and soluble carbohydrates, which appeared more prominently in the latter. These differences are entirely associated with the optimal environmental factors for the development of each phase, primarily due to their location in the water column and consequently the intensity of received light energy. Based on the data obtained in this study, a better understanding of the photosynthetic and biochemical characteristics associated with each stage of *P. linearis* development, particularly the conchocelis phase, which lacked data, is achieved. Based on the present findings, it is evident that the conchocelis phase is not an ideal source for the production and extraction of BACs when compared to the blade phase. However, it remains a critical stage in the life cycle of *Porphyra*. Future research should focus on optimizing cultivation conditions for the conchocelis phase, particularly by identifying light quality and intensity (with the present study the optimal limits are known: 43.16 [Ek_{ETR}] to 193.72 [$Eopt_{ETR}$] μmol photons·m^{-2} s^{-1}), nutrient availability, and temperature ranges that enhance its growth and transition to the blade phase. Additionally, studies investigating potential biotechnological applications of conchocelis-derived compounds (especially soluble carbohydrates) and the genetic regulation of phase transitions could provide further insights into improving large-scale production strategies. Understanding these factors is essential for maintaining continuous cultivation, ensuring year-round biomass production, and supporting the commercial exploitation of this economically valuable algae.

Supplementary Materials: The following supporting information can be downloaded at: https://www.mdpi.com/article/10.3390/phycology5010009/s1, Table S1: The t-value, *p*-value and d-value (Cohen's test) obtained after the data were analysed using the independent-samples *t*-test ($p \leq 0.05$).

Author Contributions: Conceptualization, D.T.P. and F.L.F.; Methodology, D.T.P. and F.L.F.; Investigation, D.T.P. and F.L.F.; Writing, D.T.P. and F.L.F.; Review, D.T.P. and F.L.F.; Editing—original draft preparation, D.T.P. and F.L.F.; Project administration, D.T.P. and F.L.F.; Supervision, F.L.F. All authors have read and agreed to the published version of the manuscript.

Funding: This research was funded by the European Union ('NUVAPY-BLUE' HORIZON-MSCA-2022-101106349) and by the Ministry of Science and Innovation of Spanish Government (Project 'AlgaHub: Algae for more sustainable and healthy functional foods' TED2021-131555B-C22). The first author is funded by the European Union under the Marie Sklodowska-Curie grant agreement No. 101106349. Views and opinions expressed are, however, those of the author(s) only and do not necessarily reflect those of the European Union or the European Commission (granting authority). Neither the European Union nor the granting authority can be held responsible for them.

Institutional Review Board Statement: Not applicable.

Informed Consent Statement: Not applicable.

Data Availability Statement: All data generated or analyzed during this study are included in this published article.

Acknowledgments: The authors thank the Porto Muiños company for the harvesting of *Porphyra linearis* in Galicia (Northwest Spain), as well as the Laboratory of Fotobiología y Biotecnología de Organismos Acuáticos (RNM-295, FYBOA) and the University Institute of Blue Biotechnology and Development at Grice Hutchinson Research Center (IBYDA-UMA) for providing the facilities to conduct the experiments and analyses.

Conflicts of Interest: The authors declare no conflicts of interest. All authors certify that they have no affiliations with or involvement in any organization or entity with any financial interest or non-financial interest in the subject matter or materials discussed in this manuscript.

References

1. Chan, C.X.; Zäuner, S.; Wheeler, G.; Grossman, A.R.; Prochnik, S.E.; Blouin, N.A.; Zhuang, Y.; Benning, C.; Berg, G.M.; Yarish, C.; et al. Analysis of *Porphyra* membrane transporters demonstrates gene transfer among photosynthetic eukaryotes and numerous sodium-coupled transport systems. *Plant Physiol.* **2012**, *158*, 2001–2012. [CrossRef] [PubMed]
2. Li, J.; Cui, G.; Liu, Y.; Wang, Q.; Gong, Q.; Gao, X. Effects of desiccation, water velocity, and nitrogen limitation on the growth and nutrient removal of *Neoporphyra haitanensis* and *Neoporphyra dentata* (Bangiales, Rhodophyta). *Water* **2021**, *13*, 2745. [CrossRef]
3. Blouin, N.A.; Brodie, J.A.; Grossman, A.C.; Xu, P.; Brawley, S.H. *Porphyra*: A marine crop shaped by stress. *Trends Plant Sci.* **2011**, *16*, 29–37. [CrossRef]
4. Pereira, D.T.; Batista, D.; Filipin, E.P.; Bouzon, Z.L.; Simioni, C. Effects of ultraviolet radiation (UVA+ UVB) on germination of carpospores of the red macroalga *Pyropia acanthophora* var. *brasiliensis* (Rhodophyta, Bangiales): Morphological changes. *Photochem. Photobiol.* **2019**, *95*, 803–811. [CrossRef]
5. Venkatraman, K.L.; Mehta, A. Health benefits and pharmacological effects of *Porphyra* species. *Plant Foods Hum. Nutr.* **2019**, *74*, 10–17. [CrossRef]
6. Zhou, C.; Yu, X.; Zhang, Y.; He, R.; Ma, H. Ultrasonic degradation, purification and analysis of structure and antioxidant activity of polysaccharide from *Porphyra yezoensis* Udea. *Carbohydr. Polym.* **2012**, *87*, 2046–2051. [CrossRef]
7. Guedes, É.A.; Silva, T.G.D.; Aguiar, J.S.; Barros, L.D.D.; Pinotti, L.M.; Sant'Ana, A.E. Cytotoxic activity of marine algae against cancerous cells. *Ver. Bras. Farmacogn.* **2013**, *23*, 668–673. [CrossRef]
8. Mercurio, D.G.; Wagemaker, T.A.L.; Alves, V.M.; Benevenuto, C.G.; Gaspar, L.R.; Campos, P.M. In vivo photoprotective effects of cosmetic formulations containing UV filters, vitamins, *Ginkgo biloba* and red algae extracts. *J. Photochem. Photobiol. B* **2015**, *153*, 121–126. [CrossRef]
9. Morais, T.; Cotas, J.; Pacheco, D.; Pereira, L. Seaweeds compounds: An ecosustainable source of cosmetic ingredients? *Cosmetics* **2021**, *8*, 8. [CrossRef]
10. Vega, J.; Schneider, G.; Moreira, B.R.; Herrera, C.; Bonomi-Barufi, J.; Figueroa, F.L. Mycosporine-like amino acids from red macroalgae: UV-photoprotectors with potential cosmeceutical applications. *Appl. Sci.* **2021**, *11*, 5112. [CrossRef]
11. Figueroa, F.L.; Aguilera, J.; Niell, F.X. Red and blue light regulation of growth and photosynthetic metabolism in *Porphyra umbilicalis* (L.) Kützing (Bangiales, Rhodophyta). *Eur. J. Phycol.* **1995**, *30*, 11–18. [CrossRef]

12. Korbee, N.; Huovinen, P.; Figueroa, F.L.; Aguilera, J.; Karsten, U. Availability of ammonium influences photosynthesis and the accumulation of mycosporine-like amino acids in two *Porphyra* species (Bangiales, Rhodophyta). *Mar. Biol.* **2005**, *146*, 645–654. [CrossRef]
13. Xu, P.; Chukhutsina, V.U.; Nawrocki, W.J.; Schansker, G.; Bielczynski, L.W.; Lu, Y.; Karcher, D.; Bock, R.; Croce, R. Photosynthesis without β-carotene. *eLife* **2020**, *9*, e58984. [CrossRef] [PubMed]
14. Tala, F.; Chow, F. Ecophysiological characteristics of *Porphyra* spp. (Bangiophyceae, Rhodophyta): Seasonal and latitudinal variations in northern-central Chile. *J. Appl. Phycol.* **2014**, *26*, 2159–2171. [CrossRef]
15. Pereira, D.T.; Schmidt, É.C.; Filipin, E.P.; Pilatti, F.K.; Ramlov, F.; Maraschin, M.; Bouzon, Z.L.; Simioni, C. Effects of ultraviolet radiation on the morphophysiology of the macroalga *Pyropia acanthophora* var. *brasiliensis* (Rhodophyta, Bangiales) cultivated at high concentrations of nitrate. *Acta Physiol. Plant* **2020**, *42*, 61. [CrossRef]
16. Schneider, G.; Figueroa, F.L.; Vega, J.; Chaves, P.; Álvarez-Gómez, F.; Korbee, N.; Bonomi-Barufi, J. Photoprotection properties of marine photosynthetic organisms grown in high ultraviolet exposure areas: Cosmeceutical applications. *Algal Res.* **2020**, *49*, 101956. [CrossRef]
17. Uribe, E.; Vega-Gálvez, A.; García, V.; Pastén, A.; Rodríguez, K.; López, J.; Scala, K.D. Evaluation of physicochemical composition and bioactivity of a red seaweed (*Pyropia orbicularis*) as affected by different drying technologies. *Dry. Technol.* **2020**, *38*, 1218–1230. [CrossRef]
18. Ferreira, J.; Hartmann, A.; Martins-Gomes, C.; Nunes, F.M.; Souto, E.B.; Santos, D.L.; Abreu, H.; Pereira, R.; Pacheco, M.; Galvão, I.; et al. Red seaweeds strengthening the nexus between nutrition and health: Phytochemical characterization and bioactive properties of *Grateloupia turuturu* and *Porphyra umbilicalis* extracts. *J. Appl. Phycol.* **2021**, *33*, 3365–3381. [CrossRef]
19. Kim, J.H.; Choi, S.J.; Lee, S. Effects of temperature and light on photosynthesis and growth of red alga *Pyropia dentata* (Bangiales, Rhodophyta) in a conchocelis phase. *Aquaculture* **2019**, *505*, 167–172. [CrossRef]
20. Ma, J.; Xu, T.; Bao, M.; Zhou, H.; Zhang, T.; Li, Z.; Gao, G.; Li, X.; Xu, J. Response of the red algae *Pyropia yezoensis* grown at different light intensities to CO2-induced seawater acidification at different life cycle stages. *Algal Res.* **2020**, *49*, 101950. [CrossRef]
21. Pimentel, F.B.; Machado, M.; Cermeño, M.; Kleekayai, T.; Machado, S.; Rego, A.M.; Abreu, M.H.; Alves, R.C.; Oliveira, M.B.P.P.; Fitz, G.R.J. Enzyme-assisted release of antioxidant peptides from *Porphyra dioica* conchocelis. *Antioxidants* **2021**, *10*, 249. [CrossRef] [PubMed]
22. Khan, M.N.; Mohammad, F. Eutrophication: Challenges and solutions. In *Eutroph: Causes, Consequences and Control*; Springer: Berlin/Heidelberg, Germany, 2014; Volume 2, pp. 1–15. [CrossRef]
23. Goecke, F.; Imhoff, J.F. Microbial biodiversity associated with marine macroalgae and seagrasses. In *Marine Macrophytes as Foundation Species*, 1st ed.; Ólafsson, E., Ed.; Taylor & Francis Group: Boca Raton, FL, USA, 2016; pp. 3–5.
24. Blouin, N.; Xiugeng, F.; Peng, J.; Yarish, C.; Brawley, S.H. Seeding nets with neutral spores of the red alga *Porphyra umbilicalis* (L.) Kützing for use in integrated multi-trophic aquaculture (IMTA). *Aquaculture* **2007**, *270*, 77–91. [CrossRef]
25. Kim, J.K.; Kraemer, G.P.; Neefus, C.D.; Chung, I.K.; Yarish, C. Effects of temperature and ammonium on growth, pigment production and nitrogen uptake by four species of *Porphyra* (Bangiales, Rhodophyta) native to the New England coast. *J. Appl. Phycol.* **2007**, *19*, 431–440. [CrossRef]
26. Redmond, S.; Green, L.; Yarish, C.; Kim, J.; Neefus, C. *New England Seaweed Culture Handbook: Nursery Systems*, 1st ed.; Connecticut Sea Grant: Groton, CT, USA, 2014; pp. 54–63.
27. Gheysen, L.; Demets, R.; Devaere, J.; Bernaerts, T.; Goos, P.; Van Loey, A.; Foubert, I. Impact of microalgal species on the oxidative stability of n-3 LC-PUFA enriched tomato puree. *Algal Res.* **2019**, *40*, 101502. [CrossRef]
28. Sampath-Wiley, P.; Neefus, C.D. An improved method for estimating R-phycoerythrin and R-phycocyanin contents from crude aqueous extracts of *Porphyra* (Bangiales, Rhodophyta). *J. Appl. Phycol.* **2007**, *19*, 123–129. [CrossRef] [PubMed]
29. Folin, O.; Ciocalteu, V. On tyrosine and tryptophane determinations in proteins. *J. Biol. Chem.* **1927**, *73*, 627–650. [CrossRef]
30. Umbreit, W.W.; Burris, R.H. Method for glucose determination and other sugars. In *Manome-Tric Techniques*, 1st ed.; Burgess Publishing Co.: Clayton, NC, USA, 1964.
31. Bradford, M.M. A rapid and sensitive method for the quantitation of microgram quantities of protein utilizing the principle of protein-dye binding. *Anal. Biochem.* **1976**, *72*, 248–254. [CrossRef]
32. Peinado, N.K.; Abdala-Díaz, R.T.; Figueroa, F.L.; Helbling, E.W. Ammonium and UV radiation stimulate the accumulation of mycosporine-like amino acids in *Porphyra columbina* (Rhodophyta) from Patagonia, Argentina. *J. Phycol.* **2004**, *40*, 248–259. [CrossRef]
33. Chaves-Peña, P.; De La Coba, F.; Figueroa, F.L.; Korbee, N. Quantitative and qualitative HPLC analysis of mycosporine-like amino acids extracted in distilled water for cosmetical uses in four Rhodophyta. *Mar. Drugs* **2020**, *18*, 27. [CrossRef]
34. Vega, J.; Bárcenas-Pérez, D.; Fuentes-Ríos, D.; López-Romero, J.M.; Hrouzek, P.; Figueroa, F.L.; Cheel, J. Isolation of mycosporine-like amino acids from red macroalgae and a marine lichen by high-performance countercurrent chromatography: A strategy to obtain biological UV-filters. *Mar. Drugs* **2023**, *21*, 357. [CrossRef]

35. Karsten, U.; Sawall, T.; Hanelt, D.; Bischof, K.; Figueroa, F.L.; Flores-Moya, A.; Wiencke, C. An inventory of UV-absorbing mycosporine-like amino acids in macroalgae from polar to warm-temperate regions. *Bot. Mar.* **1998**, *41*, 443–453. [CrossRef]
36. La Barre, S.; Roullier, C.; Boustie, J. Mycosporine-like amino acids (MAAs) in biological photosystems. In *Outstanding Marine Molecules*; Wiley-VCH Verlag GmbH & Co. KgaA: Weinheim, Germany, 2014.
37. Re, R.; Pellegrini, N.; Proteggente, A.; Pannala, A.; Yang, M.; Rice-Evans, C. Antioxidant activity applying an improved ABTS radical cation decolorization assay. *Free Radic. Biol. Med.* **1999**, *26*, 1231–1237. [CrossRef] [PubMed]
38. Schreiber, U.; Endo, T.; Mi, H.; Asada, K. Quenching analysis of chlorophyll fluorescence by the saturation pulse method: Particular aspects relating to the study of eukaryotic algae and cyanobacteria. *Plant Cell Physiol.* **1995**, *36*, 873–882. [CrossRef]
39. Vega, J.; Moreira, B.R.; Avilés, A.; Bonomi-Barufi, J.; Figueroa, F.L. Short-term effects of light quality, nutrient concentrations and emersion on the photosynthesis and accumulation of bioactive compounds in *Pyropia leucosticta* (Rhodophyta). *Algal Res.* **2024**, *81*, 103555. [CrossRef]
40. Figueroa, F.L.; Escassi, L.; Pérez-Rodríguez, E.; Korbee, N.; Giles, A.D.; Johnsen, G. Effects of short-term irradiation on photoinhibition and accumulation of mycosporinelike amino acids in sun and shade species of the red algal genus *Porphyra*. *J. Photochem. Photobiol. B* **2003**, *69*, 21–30. [CrossRef]
41. Figueroa, F.L.; Domínguez-González, B.; Korbee, N. Vulnerability and acclimation to increased UVB radiation in three intertidal macroalgae of different morpho-functional groups. *Mar. Environm. Res.* **2014**, *97*, 30–38. [CrossRef]
42. Eilers, P.H.C.; Peeters, J.C.H. A model for the relationship between light intensity and the rate of photosynthesis in phytoplankton. *Ecol. Model.* **1988**, *42*, 199–215. [CrossRef]
43. Parmar, A.; Singh, N.K.; Dhoke, R.; Madamwar, D. Influence of light on phycobiliprotein production in three marine cyanobacterial cultures. *Acta Physiol. Plant* **2013**, *35*, 1817–1826. [CrossRef]
44. Hu, X.; Gu, T.; Khan, I.; Zada, A.; Jia, T. Research progress in the interconversion, turnover and degradation of chlorophyll. *Cells* **2021**, *10*, 3134. [CrossRef]
45. Jiang, H.; Gao, K. Effects of UV radiation on the photosynthesis of conchocelis of *Porphyra haitanensis* (Bangiales, Rhodophyta). *Phycologia* **2008**, *47*, 241–248. [CrossRef]
46. Pereira, D.T.; Korbee, N.; Vega, J.; Figueroa, F.L. Advancing *Porphyra linearis* (Rhodophyta, Bangiales) culture: Low cost artificial seawater, nitrate supply, photosynthetic activity and energy dissipation. *J. Appl. Phycol.* **2024**, *36*, 3509–3523. [CrossRef]
47. Lin, R.; Stekoll, M. Responses of chlorophyll a content for conchocelis phase of Alaskan *Porphyra* (Bangiales, Rhodophyta) species to environmental factors. *Adv. Biosci. Bioeng.* **2013**, *1*, 28–39. [CrossRef]
48. Aple, K.; Hirt, H. Reactive oxygen species, metabolism, oxidative stress, and signal transduction. *Ann. Rev. Plant Biol.* **2004**, *55*, 373–399. [CrossRef]
49. Kottuparambil, S.; Shin, W.; Brown, M.T.; Han, T. UV-B affects photosynthesis, ROS production and motility of the freshwater flagellate, *Euglena agilis* Carter. *Aquat. Toxicol.* **2012**, *122*, 206–213. [CrossRef] [PubMed]
50. Dall'Osto, L.; Lico, C.; Alric, J.; Giuliano, G.; Havaux, M.; Bassi, R. Lutein is needed for efficient chlorophyll triplet quenching in the major LHCII antenna complex of higher plants and effective photoprotection in vivo under strong light. *BMC Plant Biol.* **2006**, *6*, 32. [CrossRef]
51. Solovchenko, A.E.; Khozin-Goldberg, I.; Didi-Cohen, S.; Cohen, Z.; Merzlyak, M.N. Effects of light and nitrogen starvation onthe content and composition of carotenoids of the green microalga *Parietochloris incisa*. *Russ. J. Plant Physiol.* **2008**, *55*, 455–462. [CrossRef]
52. Vaquero, I.; Mogedas, B.; Ruiz-Domínguez, M.C.; Vega, J.M.; Vílchez, C. Light-mediated lutein enrichment of an acid environment microalga. *Algal Res.* **2014**, *6*, 70–77. [CrossRef]
53. Gayathri, S.; Rajasree, S.R.; Suman, T.Y.; Aranganathan, L.; Thriuganasambandam, R.; Narendrakumar, G. Induction of β, ε-carotene-3, 3′-diol (lutein) production in green algae *Chlorella salina* with airlift photobioreactor: Interaction of different aeration and light-related strategies. *Biomass Convers. Biorefinery* **2021**, *11*, 2003–2012. [CrossRef]
54. Koizumi, J.; Takatani, N.; Kobayashi, N.; Mikami, K.; Miyashita, K.; Yamano, Y.; Wada, A.; Maoka, T.; Hosokawa, M. Carotenoid profiling of a red seaweed *Pyropia yezoensis*: Insights into biosynthetic pathways in the order Bangiales. *Mar. Drugs* **2018**, *16*, 426. [CrossRef] [PubMed]
55. Talarico, L.; Maranzana, G. Light and adaptive responses in red macroalgae: An overview. *J. Photochem. Photobiol. B* **2000**, *56*, 1–11. [CrossRef]
56. Fratelli, C.; Burck, M.; Amarante, M.C.A.; Braga, A.R.C. Antioxidant potential of nature's "something blue": Something new in the marriage of biological activity and extraction methods applied to C-phycocyanin. *Trends Food Sci. Technol.* **2021**, *107*, 309–323. [CrossRef]
57. Ismail, G.A.; El-Sheekh, M.M.; Samy, R.M.; Gheda, S.F. Antimicrobial, antioxidant, and antiviral activities of biosynthesized silver nanoparticles by phycobiliprotein crude extract of the cyanobacteria *Spirulina platensis* and *Nostoc linckia*. *Bionanoscience* **2021**, *11*, 355–370. [CrossRef]
58. Talarico, L. Phycobiliproteins and phycobilisomes in red algae: Adaptive responses to light. *Sci. Mar.* **1996**, *60*, 205–222.

59. Tsekos, I.; Niell, F.X.; Aguilera, J.; López-Figueroa, F.; Delivopoulos, S.G. Ultrastructure of the vegetative gametophytic cells of *Porphyra leucosticta* (Rhodophyta) grown in red, blue and green light. *Phycol. Res.* **2002**, *50*, 251–264. [CrossRef]
60. Ma, R.; Lu, F.; Bi, Y.; Hu, Z. Effects of light intensity and quality on phycobiliprotein accumulation in the cyanobacterium *Nostoc sphaeroides* Kützing. *Biotechnol. Lett.* **2015**, *37*, 1663–1669. [CrossRef] [PubMed]
61. Shick, J.M.; Dunlap, W.C. Mycosporine-like amino acids and related gadusols: Biosynthesis, accumulation, and UV-protective functions in aquatic organisms. *Ann. Rev. Physiol.* **2002**, *64*, 223–262. [CrossRef]
62. Raj, S.; Kuniyil, A.M.; Sreenikethanam, A.; Gugulothu, P.; Jeyakumar, R.B.; Bajhaiya, A.K. Microalgae as a source of mycosporine-like amino acids (MAAs); advances and future prospects. *Int. J. Environ. Res. Public Health* **2021**, *18*, 12402. [CrossRef] [PubMed]
63. Huovinen, P.; Gomez, I.; Figueroa, F.L.; Ulloa, N.; Morales, V.; Lovengreen, C. Ultraviolet-absorbing mycosporine-like amino acids in red macroalgae from Chile. *Bot. Mar.* **2004**, *47*, 21–29. [CrossRef]
64. Pereira, D.T.; Korbee, N.; Vega, J.; Figueroa, F.L. The role of nitrate supply in bioactive compound synthesis and antioxidant activity in the cultivation of *Porphyra linearis* (Rhodophyta, Bangiales) for future cosmeceutical and bioremediation applications. *Mar. Drugs* **2024**, *22*, 222. [CrossRef]
65. Amsler, C.D.; Fairhead, V.A. Defensive and sensory chemical ecology of brown algae. *Adv. Bot. Res.* **2006**, *43*, 1–91. [CrossRef]
66. Wang, H.; Ki, J.S. Molecular identification, differential expression and protective roles of iron/manganese superoxide dismutases in the green algae *Closterium ehrenbergii* against metal stress. *Eur. J. Protistol.* **2020**, *74*, 125689. [CrossRef] [PubMed]
67. Fernández-Segovia, I.; Lerma-García, M.J.; Fuentes, A.; Barat, J.M. Characterization of Spanish powdered seaweeds: Composition, antioxidant capacity and technological properties. *Food Res. Int.* **2018**, *111*, 212–219. [CrossRef] [PubMed]
68. Frei, E.; Preston, R.D. Non-cellulosic structural polysaccharides in algal cell walls-II. Association of xylan and mannan in *Porphyra umbilicalis*. *Proc. R. Soc. Lond. Ser. B Biol. Sci.* **1964**, *160*, 314–327. [CrossRef]
69. Siegel, B.Z.; Siegel, S.M. The chemical composition of algal cell walls. *Crit. Rev. Microbiol.* **1973**, *3*, 1–26. [CrossRef] [PubMed]
70. Baldan, B.; Andolfo, P.; Navazio, L.; Tolomio, C.; Mariani, P. Cellulose in algal cell wall, an "in situ" localization. *Eur. J. Histochem.* **2001**, *45*, 51–56. [CrossRef]
71. Hemmingson, J.Á.; Nelson, W.A. Cell wall polysaccharides are informative in *Porphyra* species taxonomy. *J. Appl. Phycol.* **2002**, *14*, 357–364. [CrossRef]
72. Cao, J.; Wang, J.; Wang, S.; Xu, X. *Porphyra* species: A mini-review of its pharmacological and nutritional properties. *J. Med. Food* **2016**, *19*, 111–119. [CrossRef] [PubMed]
73. Pereira, D.T.; Ouriques, L.C.; Bouzon, Z.L.; Simioni, C. Effects of high nitrate concentrations on the germination of carpospores of the red seaweed *Pyropia acanthophora* var. brasiliensis (Rhodophyta, Bangiales). *Hydrobiologia* **2020**, *847*, 217–228. [CrossRef]
74. Figueroa, F.L.; Bonomi-Barufi, J.; Celis-Plá, P.S.; Nitschke, U.; Arenas, F.; Connan, S.; Abreu, M.H.; Malta, E.J.; Conde-Álvarez, R.; Chow, F.; et al. Short-term effects of increased CO_2, nitrate and temperature on photosynthetic activity in *Ulva rigida* (Chlorophyta) estimated by different pulse amplitude modulated fluorometers and oxygen evolution. *J. Exp. Bot.* **2021**, *72*, 491–509. [CrossRef] [PubMed]
75. Figueroa, F.L.; Celis-Plá, P.S.; Martínez, B.; Korbee, N.; Trilla, A.; Arenas, F. Yield losses and electron transport rate as indicators of thermal stress in *Fucus serratus* (Ochrophyta). *Algal Res.* **2019**, *41*, 101560. [CrossRef]
76. Figueroa, F.L.; Salles, S.; Aguilera, J.; Jiménez, C.; Mercado, J.; Viñegla, B.; Flores-Moya, A.; Altamirano, M. Effects of solar radiation on photoinhibition and pigmentation in the red alga *Porphyra leucosticta*. *Mar. Ecol. Prog. Ser.* **1997**, *151*, 81–90. [CrossRef]
77. Häder, D.P.; Gröniger, A.; Hallier, C.; Lebert, M.; Figueroa, F.L.; Jiménez, C. Photoinhibition by visible and ultraviolet radiation in the red macroalga *Porphyra umbilicalis*. *Plant Ecol.* **2000**, *145*, 351–358. [CrossRef]
78. Figueroa, F.L.; Gómez, I. Photoacclimation to solar UV radiation in red macroalgae. *J. Appl. Phycol.* **2001**, *13*, 235–248. [CrossRef]